

A High-Voltage Compliant Neural Stimulator With HF Wireless Power and UHF Backscatter Communication

Vaishnavi Ranganathan¹, Brody Mahoney¹, Eric Pepin¹, Michael D. Sunshine³, Chet T. Moritz³, Jacques C. Rudell¹ and Joshua R. Smith^{2,1}

[1]Electrical Engineering [2]Computer Science and Engineering [3]Rehabilitation Medicine
University of Washington; Seattle, WA 98195

Abstract—A dual-band wireless neural stimulation device with high frequency (HF) wireless power transfer (WPT) at 13.56MHz and ultra high frequency (UHF) backscatter communication (BSC) at 915MHz is presented. Neural interfaces hold great promise in the development of future treatment/therapy for debilitating neurological disorders, spinal cord damage, and loss of limb function. Most state-of-the-art wireless neural interfaces use either HF or UHF for both WPT and communication, with UHF used in low power systems (neural recording systems) and HF in high power systems (neuromodulation systems). In contrast, this work demonstrates the efficient use of two separate frequencies for WPT and communication, with negligible interference between the two. The higher signal strength of received power using HF WPT enables the implementation of high-voltage (HV) electrical stimulation which is critical (and typically battery-powered) for treatment-oriented neuromodulation devices. Simultaneously, BSC provides improved bi-directional communication data-rates and reduced power consumption, compared to typical active radios. The wireless stimulator has been implemented on a printed circuit board (PCB) using custom and off-the-shelf discrete parts. Measurements are provided demonstrating the efficiency of simultaneously operating WPT and BSC interfaces. The results of *in vivo* measurements (anesthetized rat) demonstrating the efficacy of the wirelessly-powered stimulator are also provided.

I. INTRODUCTION

Wireless power and control have become a necessity for implanted devices, so as to improve implant lifetime and user comfort by eliminating batteries and trans-cutaneous cables. With the success of FDA-approved devices like deep-brain-stimulators and vagus nerve stimulators, there has been a growing interest in developing fully wireless/implantable neural interface devices for medical/neuroprosthetic applications [1]. Existing wireless neural interfaces either operate in the high-power domain ($\geq 100\text{mW}$), requiring near-field HF WPT, or in the low-power domain ($\sim 10\text{mW}$) which allows harvesting energy from far-field UHF signals [2]. While neural recording typically operates at low power ($\leq 50\mu\text{W}/\text{channel}$) electrical stimulation often requires high power ($\geq 1\text{mW}/\text{channel}$). Such systems need to drive current pulses (orders of $10\mu\text{A}$ to 10mA), at high-voltage compliance (i.e. $\geq \pm 10\text{V}$), through interfacing electrodes in order to modulate neural activity at desired levels in the targeted tissue. At the same time, implanted systems that incorporate both neural signal recording and stimulation are increasingly desired, with the former requiring low-power and high data-rate communication. Of specific interest are bi-directional brain computer interface (BBCI) systems which modulate the activity of neurons in response to the content of recorded neural signals. Such devices could revolutionize the treatment of limb paralysis caused

by spinal cord injury, by creating an artificial bypass across the break through post-injury stimulation (intra/epi-dural/sub-dural spinal stimulation) [3] [4]. Furthermore, the BCI can be used to record neural signals at the periphery or spinal cord and perform stimulation to restore the sensory pathway after an injury. Specifically, to support electrical stimulation for intra-spinal, epi-dural spinal and sub-dural cortical stimulation, current levels ranging from hundreds of μA to several tens of mA are necessary at HV compliance. Unavoidable loss in the front-end electronics driving the stimulus current further increases stimulator power consumption.

This work presents a dual-band, HV-compliant ($\pm 30\text{V}$) neural stimulator, with near-field WPT at 13.56MHz and BSC at 915MHz. Recent work on dual-band power and communication demonstrates high data-rate communication for a system with fixed distance between transmitter (TX) and receiver (RX) [5] [6]. The work in [2] presents WPT at 915MHz for low current ($116\mu\text{A}$) stimulation but uses a battery for higher currents since harvesting high power is challenging at 915MHz. [6] also features an integrated version of a dual-band stimulator for seizure control ($\leq 3\text{mW}$); however, its stimulation capacity is limited to 10V and $30\mu\text{A}$ and it uses active communication in the 401-406MHz band (lower data rate). In contrast, the system discussed in this paper is capable of delivering power on the order of 70mW ($\leq 0.5^\circ\text{C}$ tissue heating) with simultaneous bi-directional BSC and HV neuromodulation. The BSC front-end currently uses a radio frequency identification (RFID) protocol with 64kbps data-rates; improved data-rates can be achieved using custom protocols that run in software. Future expansion of this system to include neural recording and out-of-implant transmission of data will benefit from high data-rate provided by the 915MHz communication. A system-level description of the neural stimulator is provided in Section II, followed by a discussion on how the wireless system specifications were characterized (Section III). Measurement results are provided in Section IV, including results from the *in vivo* (anesthetized rat) evaluation of the wireless stimulator.

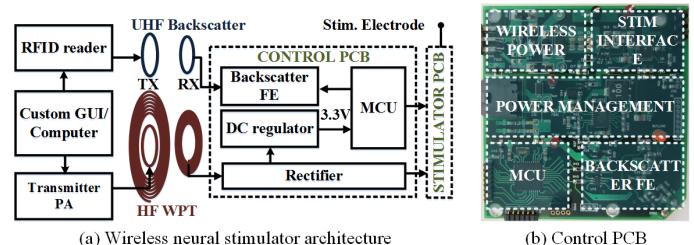


Fig. 1: a) System architecture for TX and RX, b) labeled control PCB

II. SYSTEM DESIGN

This implementation of a PCB-based stimulator is an important proof-of-concept prototype for the future development of fully-wireless (and implantable) bidirectional neural interfaces, incorporating high-power neuromodulation, low-power neural recording, and digital processing. A block-diagram of the wireless neural stimulator and the labeled prototype are provided in Fig.1. This main control PCB houses a 16-bit microcontroller unit (MCU: Texas Instruments - MSP430FR5969), which has 64kB of on-chip non-volatile FRAM memory. This prototype was designed for testability and hence is a four-layer PCB (5.2 x 5cm) with test points and components, all on the top layer. The design can be optimized to smaller form factor by populating both top and bottom layers with components and eliminating test points or by stacking smaller boards together.

A. Communication Scheme

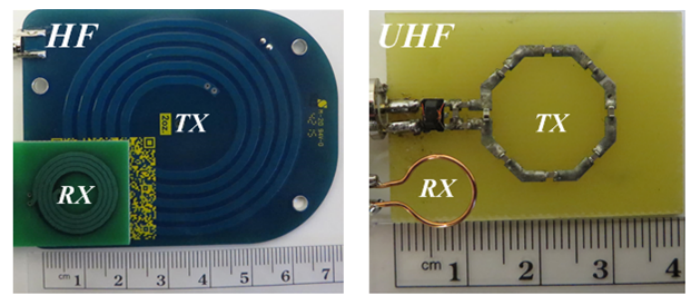
Bi-directional BSC uses a Speedway Impinj R1000 reader controlled by an interface implemented in python. The reader controller uses a Low Level Reader Protocol (LLRP) library to implement EPC Gen2 protocol [7]. Downlink (Reader to PCB) initiates communication with a 4dBm, Pulse Interval Encoded (PIE) signal and the uplink (PCB to reader) uses FM0 modulation to encode data. The receiver protocol is implemented on the MCU to recover the downlink commands from the reader. For uplink, it drives a switch across the antenna to modulate antenna impedance and scatter back the encoded data [8]. The PCB has a discrete implementation of the analog front end for BSC communication.

B. Power Management

The system uses near-field resonant WPT to meet a 70mW power budget. The receiver chain includes full-bridge rectification and DC regulation using a Linear Technology synchronous buck-boost converter (LTC3115) that can operate within an input voltage range of 2.7V to 40V. This regulator is operated in burst mode, which sets the regulator switching frequency to the minimum required to sustain the load current, thereby maintaining efficient power management across varied load conditions (i.e. stimulation loads). To compare the PCB operation while being powered by DC supply, the prototype also has an alternate path that connects a battery/DC supply to the LTC3115. A Keithley source-measure unit (SMU) was used to measure the power consumption of the PCB at a DC supply of 3.3V. The 30mW of power, required for operation of the MCU with BSC (measured with SMU at 3.3V), is dominated by the MCU power. The total power requirement of the system varies with respect to the duty-cycle of stimulation. For example, driving a 1mA, biphasic pulse stimulus at 250 μ s pulse width and 200Hz stimulus rate (i.e. 10% duty cycle) with \pm 10V compliance requires up to 1mW (depending on how capacitive the electrode-tissue interface is), plus any additional power consumption due to stimulator inefficiency. The WPT transmitter (Fig.1) employs a custom power-amplifier based on a class-E topology; this board interfaces with the external primary coil to deliver deliver 0.25W at 13.56MHz to drive it.

C. High Voltage Stimulator

The stimulator design used in this work is a HV compliant (\pm 30V), constant-current neural stimulator that is discretely implemented on a PCB using off-the-shelf HV tolerant components and a microcontroller (Fig.5a). The driver utilizes an H-bridge front-end based on the CMOS integration-compatible, high-voltage compliant topology presented in [9]. For a PCB implementation, this topology choice simplifies the power-management design and mitigates the effects of on-board parasitics on the shape of the stimulus current waveform. Specifically, it uses a single sink-regulated current DAC (IDAC) and fits within a single-supply system (VDD and GND instead of VSS, GND and VDD). It is also invariant to the resistive/capacitive (RC) nature of the electrode-tissue interface impedance. The entire biphasic stimulus is regulated by the



	HF TX	HFRX	UHF TX	UHF RX
Dia. (cm)	5.5/4.5	2	1.7	0.9
Turns	5/1	4	1	1
Type	PCB – 2oz Cu (coil/loop)	PCB – 1oz 4 layer	PCB – seg. loop	22AWG- loop

Fig. 2: Design specifications for HF and UHF coils

sinking 8-bit IDAC, configured to deliver 0-250 μ A. Rail-to-rail, slew-rate enhanced operational amplifiers (opamps) are used to supply the stimulus current. To reduce the power consumed by the stimulator (particularly at lower stimulation voltages), the high-voltage supply (HVDD) powering the opamps is provided by an ultra-low power (ULP) boost converter, which adaptively sets HVDD to be just higher than the observed average peak voltage at opamp outputs during stimulus delivery. A dedicated comparator is used to monitor the voltage at the drain of the IDAC. Lastly, the driver includes numerous switches, which are set open/closed by the microcontroller. A dual SPDT analog switch is used to multiplex the signal applied to the positive terminal of each opamp: $S_{0,C}, S_{0,D}, S_{1,C}, S_{1,D}$ and $S_{0,B}, S_{1,B}$ in Fig.5a are implemented using SPST analog switches. All the switches are tolerant to the highest output level of the opamps (30V) and can be set ON/OFF using digital signals generated by the MCU. The stimulator front-end interfaces with an active and return electrode, with large, series blocking capacitors included for safety and to enable post-stimulus charge-balancing via electrode shorting. A discrete version of the CMOS stimulator front-end topology in [9] is implemented in this work to investigate the use of this topology during *in vivo* trials and to test the ability of WPT to support HV neural stimulation. Subsequently the system is used to identify any challenges related to integrating HV stimulation with WPT and BSC on the same CMOS substrate.

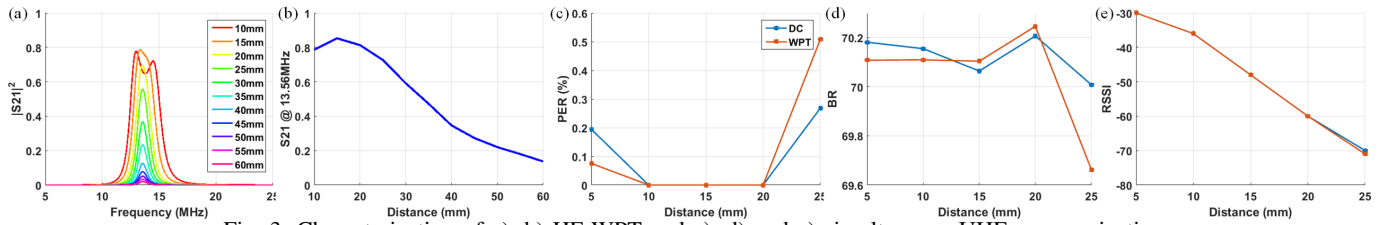


Fig. 3: Characterization of a), b) HF WPT and c), d) and e) simultaneous UHF communication

III. SYSTEM CHARACTERIZATION

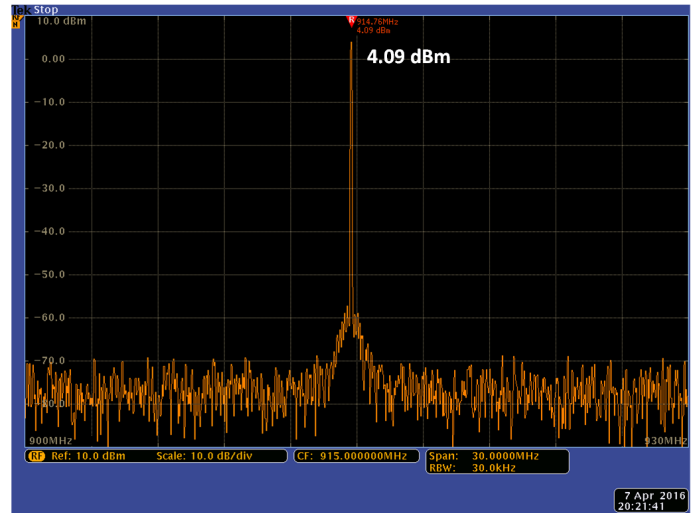
The TX and RX coils used for the following tests are shown in Fig.2, along with their design specifications. The communication front-end on the PCB is tuned using an LC-filter network to match the impedance of the loop antenna, making the S11 narrowband around 915MHz, thereby mitigating interference. The following subsections characterize WPT, BSC and the HV stimulator.

A. Wireless Power Transfer

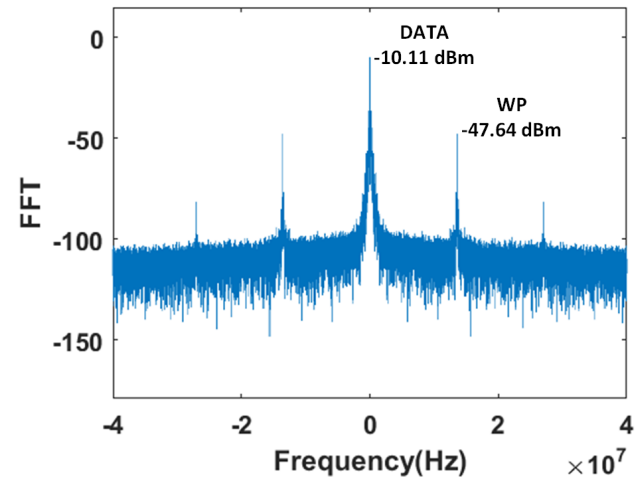
The S-parameter characterization of the two WPT coils is shown in Fig.3a, for varied distances across a frequency range of 5MHz to 25MHz. Maximum power transfer occurs at 13.56MHz for the critical and undercoupled regions. While frequency splitting is observed in the over-coupled region. Fig.3b shows the variation of WPT efficiency at 13.56MHz for varying TX-RX distances. Efficiency at the critically coupled region (10 to 20mm) is above 80% and falls off as the distance is increased, accordingly WPT can completely meet the receiver load expectations (70mW) at up to 45mm distance. A test to measure tissue heating with WPT across skin was done with the RX coil implanted in the abdomen of a sedated rat. Temperature increase was recorded in the tissue above and below the coil over a span of 7 minutes (WPT driving a 100mW load) and was measured to fall under 0.5°C. The measurement was done with thermocouples and two Fluke 287 multimeters interfaced to Labview for data logging. For this implanted measurement, the receiver test coil was coated with a biocompatible material and any detuning caused by the tissue was compensated by reducing the tuning capacitor on the receiver test coil.

B. Backscatter Communication

To characterize the BSC front-end and demonstrate simultaneous operation with WPT, the distance between communication TX and RX was varied from 5 to 25mm at a reader output power of 4dBm. A spectral plot of the UHF transmit power from the reader is plotted in Fig.4a. Power and communication TX coils were adjacently placed and the RX coils were placed facing the respective TX coil. The system was characterized by reading 32 bytes of dummy-data from the MCU for a minute. Each read command using the EPC Gen2 protocol fetches 96 bits of EPC ID and 32 bytes of data (total of 352 bits). The entire communication was logged with a custom GUI and processed using a Matlab script to extract three parameters; bit rate (BR-kbps), packet error rate (PER=failed reads/total number of reads) and received signal strength indication (RSSI);(Fig.3c-e). These parameters were obtained when the PCB was both DC powered and wirelessly powered. The first inference that can be made from (Fig.3c



(a) UHF transmit power spectrum



(b) Interference of HF on UHF

Fig. 4: Power spectrum of UHF transmit power and interference of HF on UHF data recorded post-filtering on PCB

and d) is that communication efficiency is not affected by simultaneous WPT, which is expected since any interference between the two frequency bands was made negligible by design. Secondly, PER is lower than 0.2% up to a distance of 20mm; however after 25mm the PER (BR) begin to significantly increase (decrease). The RSSI values show a linear decrease in signal strength as the receiver is moved away, with a sensitivity up to -60dBm at 20mm.

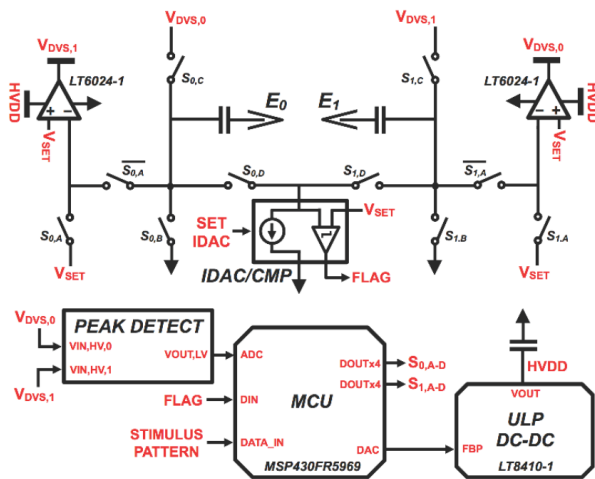
To further investigate the interference of HF power on UHF data, the spectrum from data received on the PCB, after filtering but before demodulation, was analyzed. Downlink

data was recorded with the HF power TX adjacent to the UHF TX and the FFT was obtained from the envelope. Fig.4b plots the FFT observation from which it is evident that the headroom between the two frequency bands is 37.53dBm. This reinforces the result showing similar BR and PER when the system was powered by DC and by WPT.

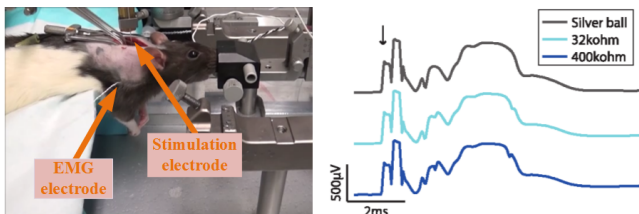
C. Neural Stimulator

The wireless neural stimulator was bench-top tested to characterize power consumption. In stand-by mode (i.e. not driving a load), the isolated stimulator PCB consumes 3.3mW to 8.5mW, when the HVDD is set at 3.5V to 24V, respectively. The entire system, including the control PCB, consumes $\sim 70\text{mW}$, in stand-by with HVDD set to 24V. To verify the stimulator operation under variable practical loading conditions, multiple RC combinations were applied as stimulus loads on a bench-top test. A current of $250\mu\text{A}$ was driven through a series combination of $2.7\text{k}\Omega$ and 2.0nF to test the response of the dynamic rails and the comparator.

IV. WIRELESS SPINAL STIMULATION



(a) Schematic of stimulation PCB



(b) EMG response to stimulation from sedated rat

Fig. 5: a) Schematic of the stimulator PCB, b) StTAs of triceps EMG response to spinal stimulation. Arrow indicates time at which stimulus was delivered.

The stimulator was programmed to deliver biphasic stimulus to the spinal cord (C6 segment) of a sedated rat to evoke muscle activity in the triceps. The system was wirelessly powered and stimulation was controlled externally using the UHF channel. Stimulus pulse-width and frequency were set to $250\mu\text{s}$ and 1Hz, respectively. The active epidural stimulation electrode was a silver ball electrode, and the intra-spinal stimulation active electrode was a single tungsten microelectrode with either $32\text{k}\Omega$ or $400\text{k}\Omega$ tip impedance measured at

1kHz. Stimulus amplitude was varied with active electrode ($32\text{k}\Omega$ or $400\text{k}\Omega$). Electromyography (EMG) activity from the triceps muscle was sampled at 24414Ks/s for offline analysis. The stimulus-triggered averages (StTAs) were recorded with a period of -1 to 9ms from the stimulus onset. The EMG data were then rectified and averaged. As shown in Fig.5b, post-stimulation, there is a clear EMG response in the targeted triceps associated with the applied stimulus. This correlated with triceps contraction in the sedated rat. The wireless stimulator was verified for reliable performance with all three investigated spinal stimulation configurations, with the capability of WPT to handle the varying load, without a drop-out in communication.

V. CONCLUSION

This work presents a dual-band wireless HV neural stimulator that benefits from HF WPT (at 13.56MHz) and UHF BSC (at 915MHz) to control stimulation externally. WPT was capable of meeting the stimulator power budget ($\sim 70\text{mW}$) up to 45mm between TX and RX with an output power of 0.25W from the external WPT transmitter and $\leq 0.5^\circ\text{C}$ heating. BSC was efficient with less than 2% PER up to a distance of 20mm, while operating simultaneously with WPT. The application of this wireless stimulator, for rehabilitation research and neuroprosthetics for spinal cord injury, was evaluated *in vivo*, in a rodent, by varying stimulation electrodes and drive strengths.

VI. ACKNOWLEDGEMENT

The authors would like to thank Zerina Kapetanovic for her assistance in setting up the communication graphical user interface. Support for project by NSF award EEC-1028725, NSF Engineering Research Center for Sensorimotor Neural Engineering

REFERENCES

- [1] H.-M. Lee, H. Park, and M. Ghovanloo, "A power-efficient wireless system with adaptive supply control for deep brain stimulation," *IEEE JSSC*, vol. 48, no. 9, pp. 2203–2216, Sept 2013.
- [2] H.-G. Rhew *et al.*, "A fully self-contained logarithmic closed-loop deep brain stimulation soc with wireless telemetry and wireless power management," *IEEE JSSC*, vol. 49, no. 10, pp. 2213–2227, Oct 2014.
- [3] S. Zanos *et al.*, "The neurochip-2: An autonomous head-fixed computer for recording and stimulating in freely behaving monkeys," *IEEE T. on Neural Systems and Rehabilitation Engineering*, vol. 19, no. 4, pp. 427–435, Aug 2011.
- [4] C. T. Moritz, S. I. Perlmutter, and E. E. Fetz, "Direct control of paralysed muscles by cortical neurons," *Nature*, vol. 456, no. 7222, pp. 639–642, 2008.
- [5] J. Besnoff, M. Abbasi, and D. Ricketts, "High data-rate communication in near-field rfid and wireless power using higher order modulation," *IEEE Transactions on MTT*, vol. 64, no. 2, pp. 401–413, Feb 2016.
- [6] W.-M. Chen *et al.*, "A fully integrated 8-channel closed-loop neural-prosthetic soc for real-time epileptic seizure control," in *IEEE ISSCC*, Feb 2013, pp. 286–287.
- [7] "Python client for LLRP-based RFID readers, howpublished = <https://github.com/ransford/sllurp>."
- [8] S. Thomas *et al.*, "A battery-free multichannel digital neural/emg telemetry system for flying insects," *Biomedical Circuits and Systems, IEEE Transactions on*, vol. 6, no. 5, pp. 424–436, Oct 2012.
- [9] E. Pepin *et al.*, "High-voltage compliant, capacitive-load invariant neural stimulation electronics compatible with standard bulk-cmos integration," in *IEEE BioCAS*, Oct 2014, pp. 260–263.